The Journal of **Immunology**

Highly Dynamic Transcriptional Signature of Distinct Macrophage Subsets during Sterile Inflammation, Resolution, and Tissue Repair

This information is current as of January 23, 2017.

Tamas Varga, Rémi Mounier, Attila Horvath, Sylvain Cuvellier, Florent Dumont, Szilard Poliska, Hamida Ardjoune, Gaëtan Juban, Laszlo Nagy and Bénédicte Chazaud

Supplementary Material	http://www.jimmunol.org/content/suppl/2016/04/29/jimmunol.1502490.DCSupplemental.html
References	This article **cites 48 articles**, 20 of which you can access for free at: http://www.jimmunol.org/content/196/11/4771.full#ref-list-1
Subscriptions	Information about subscribing to *The Journal of Immunology* is online at: http://jimmunol.org/subscriptions
Permissions	Submit copyright permission requests at: http://www.aai.org/ji/copyright.html
Email Alerts	Receive free email-alerts when new articles cite this article. Sign up at: http://jimmunol.org/cgi/alerts/etoc

Highly Dynamic Transcriptional Signature of Distinct Macrophage Subsets during Sterile Inflammation, Resolution, and Tissue Repair

Tamas Varga,*,[1] Rémi Mounier,[†,‡,§,1] Attila Horvath,* Sylvain Cuvellier,[¶,‖,#]
Florent Dumont,[¶,‖,#] Szilard Poliska,*,** Hamida Ardjoune,[¶,‖,#] Gaëtan Juban,[†,‡,§]
Laszlo Nagy,*,[††,‡‡,2] and Bénédicte Chazaud[†,‡,§,¶,2]

Macrophage gene expression determines phagocyte responses and effector functions. Macrophage plasticity has been mainly addressed in in vitro models that do not account for the environmental complexity observed in vivo. In this study, we show that microarray gene expression profiling revealed a highly dynamic landscape of transcriptomic changes of $Ly6C^{pos}CX3CR1^{lo}$ and $Ly6C^{neg}CX3CR1^{hi}$ macrophage populations during skeletal muscle regeneration after a sterile damage. Systematic gene expression analysis revealed that the time elapsed, much more than Ly6C status, was correlated with the largest differential gene expression, indicating that the time course of inflammation was the predominant driving force of macrophage gene expression. Moreover, $Ly6C^{pos}/Ly6C^{neg}$ subsets could not have been aligned to canonical M1/M2 profiles. Instead, a combination of analyses suggested the existence of four main features of muscle-derived macrophages specifying important steps of regeneration: 1) infiltrating $Ly6C^{pos}$ macrophages expressed acute-phase proteins and exhibited an inflammatory profile independent of IFN-γ, making them damage-associated macrophages; 2) metabolic changes of macrophages, characterized by a decreased glycolysis and an increased tricarboxylic acid cycle/oxidative pathway, preceded the switch to and sustained their anti-inflammatory profile; 3) $Ly6C^{neg}$ macrophages, originating from skewed $Ly6C^{pos}$ cells, actively proliferated; and 4) later on, restorative $Ly6C^{neg}$ macrophages were characterized by a novel profile, indicative of secretion of molecules involved in intercellular communications, notably matrix-related molecules. These results show the highly dynamic nature of the macrophage response at the molecular level after an acute tissue injury and subsequent repair, and associate a specific signature of macrophages to predictive specialized functions of macrophages at each step of tissue injury/repair. *The Journal of Immunology*, 2016, 196: 4771–4782.

Sterile inflammation is the response to tissue damage. After mounting inflammation to remove tissue debris, resolution of inflammation takes place to allow tissue repair. Macrophages are major players in these processes because they are involved in both mounting and resolution of inflammation, as well as in subsequent tissue repair. These multiple roles are possible due to their high versatility and plasticity (1). Macrophage plasticity has been mainly explored in vitro, where defined conditions of stimulation led to the definition of activation states. Classically activated macrophages (M1) were originally elicited by IFN-γ (then later on by LPS) and secrete proinflammatory compounds (IL-12, IL-1β, TNF-α, reactive oxygen species, and so on). Alternative activation state was first described upon IL-4 exposure. M2 macro-

phages notably express YM1, arginase 1, CCL24, and CCL17. However, a series of stimuli (glucocorticoids, TGF-β, IL-10, etc.) induce M2-like phenotypes, which overlap with each other in the expression of some genes and functions (2). Moreover, it has been recently shown that even in a controlled in vitro context, a variety of stimuli induce some intermediate phenotypes between the originally described M1 and M2 profiles (3).

In vivo analyses of macrophages used transgenic mice strains able to trace macrophage subsets, which fates and phenotypes depend on the tissue and the immune context (4–7). Tissue damage induces the infiltration of $CCR2^{pos}CX3CR1^{lo}Ly6C^{pos}$ monocytes that express proinflammatory markers. In all tissues studied so far, resolution of inflammation is associated with a shift of the inflammatory

status of macrophages that become CCR2^{neg}CX3CR1^{hi}Ly6C^{neg} (4, 5, 7). The latter sustain dampening of inflammation and tissue remodeling (1). Based on the analysis of a series of markers, the CCR2^{pos}CX3CR1^{lo}Ly6C^{pos}/CCR2^{neg}CX3CR1^{hi}Ly6C^{neg} macrophage subsets were proposed to mirror the M1/M2 in vitro paradigm. However, aligning the macrophage phenotypes observed in vivo with those described in vitro has proved difficult because of the overlapping of several markers in the in vivo populations (8). Recent studies, based on high-throughput technologies, have defined phenotypes of in vivo macrophages, but these studies have been mainly carried out in resting tissues. They defined a core signature of macrophages, helping the identification of new pan-macrophage markers, such as CD64 and merTK (9). In contrast, genomic analyses evidenced that tissue-resident macrophages isolated from a variety of tissues exhibit specific enhancer/transcriptional signature according to the tissue where they reside (10, 11). As a whole, very little information is available about the dynamics of the molecular signature of macrophages during acute inflammation and subsequent tissue repair in vivo.

We provide in this article a comprehensive analysis of the dynamics of the molecular signature of macrophages from the mounting of the immune response to the resolution of inflammation and tissue repair. For this purpose, the model of postinjury skeletal muscle regeneration, which follows a reproducible kinetics of macrophage subset transition, was used in the CX3CR1$^{GFP/+}$ mouse strain, which allows to trace macrophages (4–7, 12). Macrophage subsets were isolated at various time points of muscle regeneration and their transcriptomic profile was analyzed by microarray, defining new molecular pathways characterizing in vivo dynamics of macrophage populations during tissue repair.

Materials and Methods
Mice

CX3CR1$^{GFP/+}$ mice were bred and used according to French legislation. Experiments were conducted at 8–10 wk of age. Muscle injury was caused by i.m. injection of cardiotoxin (CTX) in the tibialis anterior muscle, as previously described (13). Muscles were harvested 1, 2, 4, and 8 d postinjury. In some experiments, CTX was coinjected with LPS (50 μg/ml final). Muscle fascia was removed; then muscles were either dissociated or frozen in nitrogen-chilled isopentane and kept at −80°C until use.

Histology

Cryosections were prepared for H&E staining and immunolabeling. Immunolabeling used anti-F4/80 (ab6640, ab74383; Abcam), Lcn2 (BAF1857; Biotechne), saa3 (provided by P.E. Scherer, Dallas, TX), and haptoglobin (ab35835; Abcam) Abs. Secondary Abs were coupled to FITC, Cy3, or Cy5 (Jackson Immunoresearch). HE-stained muscle sections were recorded with a Nikon E800 microscope at 20× magnification connected to a QIMAGING camera. Fluorescent immunolabeling was recorded with a Zeiss Axio Observer Z1 microscope connected to a Coolsnap camera at 20× magnification.

Isolation of macrophages from skeletal muscle was performed as described earlier (13) after sorting of CD45^{pos} cells and labeling with allophycocyanin-conjugated anti-Ly6C/G Abs (eBioscience), using a FACSAria III cell sorter (BD Biosciences). Cells were immediately centrifuged and RNA was extracted with the TRIzol/chloroform procedure. Validation of cell identity was assessed by flow cytometry using anti-CD64, anti-F4/80, and anti-CD103 (eBioscience) Abs.

Real-time quantitative RT-PCR

RNA was extracted from isolated CD45^{pos} cells with TRIzol/ethanol precipitation. Transcript quantification was performed by real-time quantitative RT-PCR using SYBR green assays (Ifitm6 and Serpinb2) or PrimeTime assays from IDT (Il1f9, Saa3, and S100a9). Results were analyzed with the standard delta cycle threshold method and were normalized to the expression of ActB.

Microarray processing

RNA integrity was checked on Agilent Bioanalyzer 2100, RNA samples with >9.0 RNA integrity number value were used in the downstream experiments. NanoDrop ND-1000 was used to determine RNA concen-

tration. Global expression data were obtained using Affymetrix GeneChip Mouse Gene 1.0 ST arrays. Ambion WT Expression Kit (Life Technologies) and GeneChip WT Terminal Labeling and Control Kit (Affymetrix) were used for generating biotin-labeled sense strand cDNA. The biotinylated sense strand cDNA samples were hybridized at 45°C for 16 h; then standard washing protocol was performed using Affymetrix GeneChip Fluidics Station 450, and the arrays were scanned on GeneChip Scanner 7G (Affymetrix). The microarray data are publicly available (data access: http://www.ncbi.nlm.nih.gov/geo/query/acc.cgi?acc=GSE71152).

Expression data processing and analysis

Data quality control and analysis were carried out following the recommendations put forward on the ImmGen Web site (http://www.immgen.org/Protocols/ImmGen%20QC%20Documentation_ALL-DataGeneration_0612.pdf). Data were loaded into the Genespring GX software, and robust multiarray average summarization was carried out. Next, a set of filtering steps was applied to the data set. In brief, data distribution curve was generated and the lowest 5% of the entities with detectable signals were filtered out as not expressed. Duplicate entities, not/poorly annotated transcripts and transcripts reporting inconsistent expression values were also discarded. Further analysis was carried out on the filtered data set. Data were analyzed either based on the RAW expression values or after a "per gene" normalization (individual gene expression data normalized to the median of the gene). Further analysis of gene expression and comparisons were made either within Genespring GX or using the R software package. Two-way ANOVA tests were performed in R using functions aov and Tukey HSD of package MASS. Heat maps were drawn with package pheatmap. Statistically significant difference was considered as $p < 0.05$.

Clusterization of genes according to the time

Data were robust multi-array average normalized with R/Bioconductor. Data were first controlled and analyzed in an unsupervised way by principal component analysis (PCA), and a one-way ANOVA was applied to extract DEGs using PartekGS software. Genes were selected on the global $p < 0.01$. A cluster analysis was then applied on selection by hierarchical clustering (Pearson for similarity and average for clustering) to find correlate genes. Enrichment analyses were carried out through the use of IPA and Pathway Studio software.

Comparison with previously described modules

Gene set enrichment analysis (GSEA) was performed as described previously (14) using the KEGG pathway database (http://www.genome.jp/kegg/pathway.html) as in Jha et al. (15) and for 49 gene sets associated with macrophage activation as in Xue et al. (3).

Gene ontology analysis

Lists of genes in the clusters were analyzed using DAVID tool (http://david.abcc.ncifcrf.gov/home.jsp) using at least 10 occurrences to create a gene ontology (GO). GOs with p values <0.05 were then entered together with their p value in REVIGO tool (http://revigo.irb.hr/), and results were presented according to their $\log_{10} p$ value.

Results
Experimental setup

Injection of CTX in tibialis anterior muscle of CX3CR1$^{GFP/+}$ mouse triggers damage of the whole muscle, a massive infiltration of Ly6C^{pos}CX3CR1^{lo} monocytes/macrophages, followed by a sequence of well-characterized events triggering muscle regeneration (12, 16). At day 1 after injury, myofibers were necrotic, whereas neutrophils and circulating CCR2^{pos}CX3CR1^{lo}Ly6C^{pos} monocytes enter into the damaged muscle to create Ly6C^{pos}CX3CR1^{lo} macrophages (Fig. 1). They represent the majority of macrophages at this time point (∼1800 macrophages/mg muscle [13]). At day 2, macrophages phagocyted the dead myofibers and skewing from Ly6C^{pos}CX3CR1^{lo} (hereafter Ly6C^{pos}) to Ly6C^{neg}CX3CR1^{hi} (hereafter Ly6C^{neg}) macrophages had already started (17, 18) (Fig. 1). They represent ∼5000 and 5500 macrophages/mg muscle, respectively (13). Day 4 after injury, the regeneration process was visible with the appearance of the new regenerating myofibers surrounded by numerous macrophages, which were mainly Ly6C^{neg} at this stage (∼5100 versus 750 macrophages/mg muscle [13]). At day 8, muscle
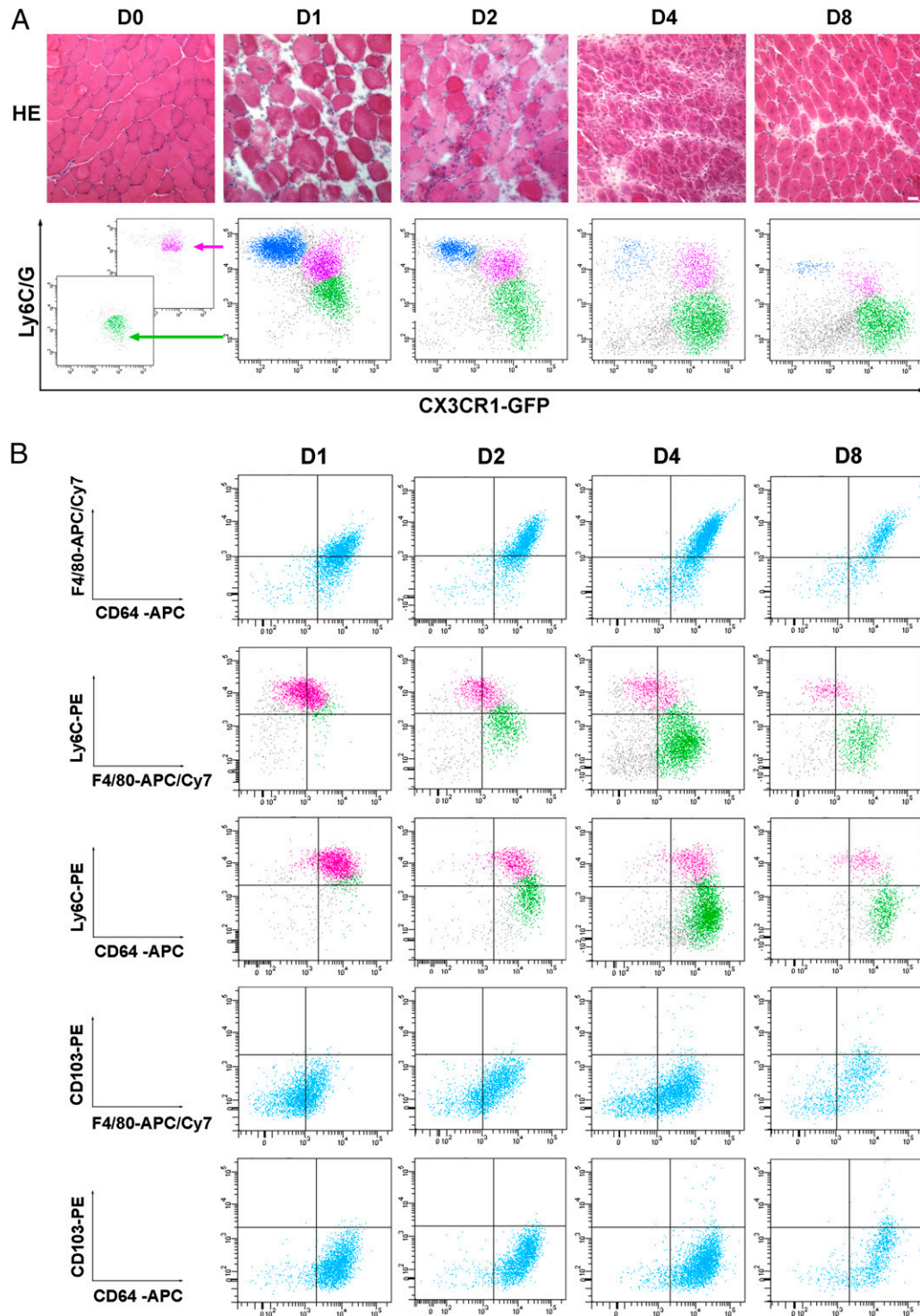
FIGURE 1. Histological characterization of muscle regeneration and macrophage sorting strategy. Tibialis anterior muscles from CX3CR1$^{GFP/+}$ mice were injected with CTX and were recovered at various days after injury. (**A**) *Top row* presents H&E staining of muscle sections. *Bottom row* presents cell sorting of CD45^{pos} cells isolated from regenerating muscle according to their Ly6C/G and GFP (CX3CR1) expression. Blue dots label Ly6C/G^{pos}CX3CR1^{neg} neutrophils. Pink dots label Ly6C^{pos}CX3CR1^{lo} macrophages. Green dots label Ly6C^{neg}CX3CR1^{hi} macrophages. Dot plots on the left give examples of the purity of sorted macrophage populations. Scale bar, 30 μm. (**B**) CD45^{pos} cells were labeled for the detection of Ly6C and for canonical macrophage (F4/80 and CD64) or DC (CD103) markers to validate the macrophagic identity of CX3CR1-(GFP)^{pos} cells. Gating is made on GFP^{pos} cells.

had almost recovered its original appearance, with neofibers characterized by the central location of their nuclei and the progressive disappearance of macrophages (600 Ly6C^{neg} macrophages/mg muscle [13]). Macrophages were sorted according to their Ly6C and CX3CR1-GFP expression. Macrophage identity of the isolated CD45^{pos}CX3CR1^{pos} muscle cells was confirmed by the almost complete overlap of CX3CR1 labeling with two macrophage markers, F4/80 and CD64, and by the absence of overlap of CX3CR1 labeling with the DC markers CD103 (Fig. 1). Pure populations (>98%) were obtained (Fig. 1) and global gene expression analysis

was performed. Because normal skeletal muscle parenchyma contains only few macrophages (12, 19), this state was not evaluated. Notably, with very few amounts of Ly6C^{pos} cells being recovered at day 8, only one point (and not triplicate) was analyzed, to avoid unethical sacrifice of numerous mice.

Muscle macrophages among other macrophage subtypes

PCA analysis of muscle macrophages versus monocytes, macrophages, and DCs sorted from various tissues and identified by the ImmGen Consortium (9, 20) revealed that muscle macrophages formed a distinguishable group (Supplemental Fig. 1A). Because a technical batch effect resulting in a similar pattern cannot be excluded, the batch removal utility of the Iimma R package (21) was used. The analysis showed that batch effects played a detectable but minor role in the PCA analysis, and that the two-dimensional PCA distribution of muscle macrophages was not altered (Supplemental Fig. 1B). We therefore suggest that the specific clustering of muscle macrophages is mostly due to their origin from a regenerating and not a resting tissue. Expression of *Ly6C* and *Cx3cr1* genes reported the expected patterns in the sorted populations and validated the sorting strategy (Fig. 2A). ImmGen proposed a list of genes that are the most specific to macrophages and classical DCs (9, 20), which was compared with muscle-derived macrophages (Supplemental Fig. 2A). Three genes (*Slamf7*, *Ass1*, and *Gpr132*) showed a DC-like expression pattern in all muscle-derived macrophages. Eighteen of the 24 classical DC genes were either not (*Rab30*, *Hmgn3*, *Gpr82*, etc.) or were weakly (*kit*, *amica1*, *ap1s3*, *pvrl1*, etc.) expressed by muscle macrophages. The three remaining genes (*CCR7*, *P2Ry10*, and *Adam19*) were upregulated in Ly6C^{neg} macrophages notably at late time points. Conversely, muscle-derived macrophages clearly expressed a core macrophage signature and clustered with macrophages sorted from other origins, and apart from DCs (Supplemental Fig. 2B). Only a few genes (*Pecr*, *Tmem195*, and *Pla2g15*) were not or were very weakly expressed.

Unique molecular signature of muscle macrophage subsets

PCA showed that macrophage populations segregated by day, more than by their LyC6$^{pos/neg}$ status (Fig. 2B). Day 1–2 macrophages clustered together, whereas day 4–8 macrophages clustered together apart, corresponding to the proinflammatory phase (days 1–2) and the resolving/regenerative phase (days 4–8) of muscle regeneration, respectively. Scatterplots of gene expression changes between macrophage subsets showed a correlation coefficient *r* value of 0.222 at day 2, indicating that the most differential transcriptional changes occurred at day 2, which corresponds to the beginning of skewing of macrophages from Ly6C^{pos} to Ly6C^{neg} phenotype (13, 22) (*r* values of 0.696, 0.756, and 0.499, for days 1, 4, and 8, respectively) (Fig. 2C). Further analysis of differential gene expression involved two-way ANOVA analysis, followed by Tukey post hoc tests ($p < 0.05$) (Supplemental Table 1). Fig. 2D shows a scheme of the comparisons made, with the number of genes showing significant differences between any two conditions. In vertical comparisons, Ly6C^{pos} were compared with Ly6C^{neg} macrophages for each time point. Confirming the earlier analyses, the highest number of differentially expressed genes was observed at day 2 of regeneration. In horizontal comparisons, each macrophage subset was compared with its closest neighboring time points to analyze variation of gene expression longitudinally along the regeneration process. The numbers of genes differentially expressed in horizontal comparisons were higher than that in vertical comparisons, confirming the PCA analyses. Thus, although Ly6C^{pos} and Ly6C^{neg} macrophages were
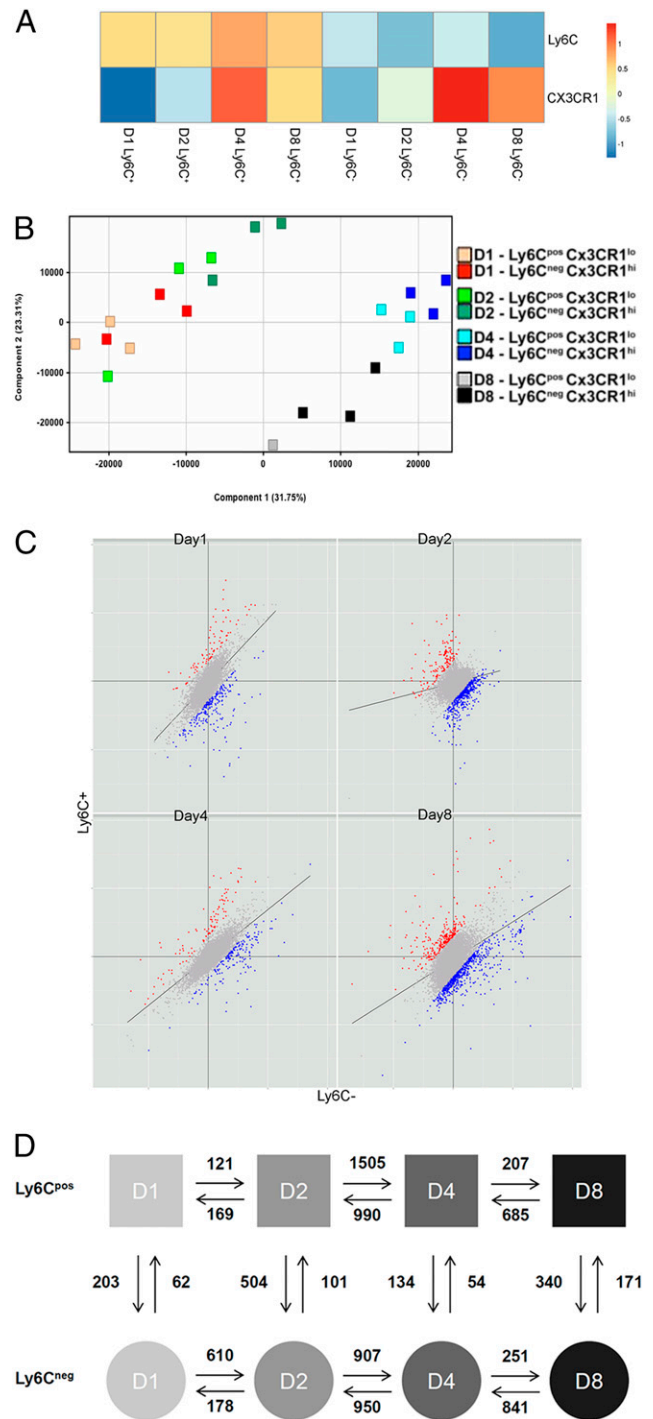
FIGURE 2. Global molecular signature of muscle macrophage subsets. (**A**) Expression of cell-surface markers used for the cell sorting strategy by Ly6C^{neg} and Ly6C^{pos} macrophages. (**B**) PCA on all muscle-derived macrophage subsets during regeneration. (**C**) Comparison of the gene expression pattern of Ly6C^{neg} and Ly6C^{pos} macrophages at different days. Scatterplots show normalized expression of each transcript of the curated entity list (positive with red; negative with blue; unchanged with gray) in Ly6C^{neg} or Ly6C^{pos} cells. Solid lines represent one-dimensional regression model with 95% CI. (**D**) Schematic of macrophage subset comparisons with two-way ANOVA analysis (see Supplemental Table 1). Numbers represent upregulated and downregulated genes between the compared conditions. Arrows point toward inductions.

different, both underwent larger transcriptomic changes during the time course of muscle regeneration, and particularly between days 2 and 4 (Fig. 2D).

Comparative analysis of Ly6C^pos and Ly6C^neg macrophage subsets

Previous studies showed that Ly6C^pos macrophages express higher levels of TNF-α and IL-1β and lower levels of TGF-β and IL-10 than Ly6C^neg macrophages (12, 16, 23). Therefore, they were considered as proinflammatory and anti-inflammatory macrophages, respectively. However, the analysis of a series of markers showed that, in general, Ly6C^pos and Ly6C^neg macrophages did not exhibit high differential expression levels of proinflammatory (M1) and anti-inflammatory (M2) markers (Fig. 3A, 3B). The difference in expression was modest and reached significance only for *Tlr4*, *IL1rap*, *IL15*, and *IL18* genes of the 23 investigated proinflammatory markers (Fig. 3A) and for 6 of the 40 anti-inflammatory genes analyzed (*Irf4*, *Ccl17*, *Ccl22*, *Ccl12*, *Clec10a*, and *Socs2*) (Fig. 3B) at day 1. These results show that Ly6C^pos and Ly6C^neg macrophages in regenerating muscle cannot be defined as canonical M1 or M2 macrophages. To refine muscle-derived macrophage subset phenotypes, we performed GSEA enrichment against the 49 modules of genes defined by Xue et al. (3), in which various combinations of these modules characterize 29 conditions of in vitro activation of human macrophages (Supplemental Table 2). Among all comparisons, only genes upregulated in Ly6C^neg macrophages at day 4 of regeneration were associated with 26 modules. The best representative combinations (Supplemental Table 2) were treatments with fatty acids (oleic, stearic, and lauric acid) and with TNF-α+Pam3CysSerLys4+PGE2, all of which triggered opposite activation status along the IFN-γ/IL-4 activation axis (3). These results indicate that, in vivo, macrophages display highly different inflammatory profiles than those previously described in vitro and from the M1/M2 nomenclature.

The expression pattern of a series of molecules secreted by macrophages and involved in myogenesis (insulin-like growth factors, urokinase plasminogen activator, platelet-derived growth factor α, hepatocyte growth factor, bone morphogenetic protein 2 [24–29]) was increased with time of regeneration, and particularly in Ly6C^neg macrophages (Fig. 3C). This shows good overlap with anticipated expression patterns of regulators of muscle regeneration. This indicated that an unbiased analysis of gene expression patterns might report yet unidentified molecular mechanisms during both acute and resolution phases of inflammation.

Comparison of Ly6C^pos and Ly6C^neg macrophage subsets during muscle regeneration

Vertical comparison between Ly6C^pos and Ly6C^neg macrophages at day 1 showed that the list of upregulated genes in Ly6C^pos macrophages (Fig. 2D, Supplemental Table 1) was enriched for GO terms associated with innate immune response and cell locomotion (Supplemental Table 3), in accordance with a role in the mounting of the inflammatory response. Strikingly, 8 of 10 of the top-ranking genes were related to inflammation (Supplemental Table 1). Thus, the "find similar entity" algorithm of the Genespring software (with similarity setting 0.5–1) was used to find genes that were regulated similarly as Il1f9, the top-ranked inflammatory gene at day 1 of muscle regeneration. Altogether, 38 genes were identified, among which 17 genes are linked to inflammation (Fig. 4A, underlined in red) and therefore constitute the best molecular signature of Ly6C^pos macrophages after a sterile muscle damage. This panel of Ly6C^pos inflammatory genes showed very good overlap with the genes identified by the GO/REVIGO approach, including alarmins (*S100a8* and *S100a9*) and several acute-phase proteins (*Lcn2*, *Lrg1*, *Hp*, and *Saa3*). The biological relevance of this expression was confirmed by the detection of haptoglobin, lipocalin-2, and

Saa3 proteins in macrophages (F4/80^pos) in early regenerating muscle (Fig. 4B).

Classical activation has been originally linked to the IFN-γ–STAT1 signaling pathway (2, 30). We showed that the IFN-γ–responsive gene, *Ifitm6*, as well as *Saa3*, *Il1f9*, *Serpinb2*, and *S100a9*, were not differentially expressed in wild-type (WT) versus STAT1 knock-out CD45^pos cells sorted from early regenerating muscle (Fig. 4C), indicating that the inflammatory profile of Ly6C^pos macrophages was not driven by IFN-γ. Nevertheless, the expression of these genes relied on a proinflammatory profile because the coinjection of CTX with LPS strongly induced their expression (Fig. 4C).

From day 2, vertical comparisons reflected the proliferative nature of Ly6C^neg muscle macrophages as they showed a high enrichment for cell cycle and cell division GOs, particularly 2 and 4 d after injury (Supplemental Table 3), confirmed by the definition of a cell cycling molecular signature of the Ly6C^neg macrophage subset (Fig. 3D), that was previously evidenced at the cell level by experiments showing that only Ly6C^neg macrophagic cells were capable of proliferation (12).

Dynamics of Ly6C^pos macrophages during the course of muscle regeneration

Ly6C^pos macrophages are the most numerous during the first steps of regeneration. From day 2, they start to switch their phenotype into Ly6C^neg cells (13) whose number gradually increases. Horizontal comparisons showed no specific GO function enrichment between days 1 and 2 of regeneration (Fig. 2D). The most important changes were observed between days 2 and 4 of regeneration when the cells showed marked differential expression of genes related to inflammation and metabolism (Supplemental Table 4). Among the upregulated genes (see top/bottom genes in Supplemental Table 1) were found a series of molecules involved in the interactions with adaptive immunity (*Cd209d*, *Cd8b1*, *Cd7*, *Ifng*, *Cd4*, *Cd3e*, *Ciita*, *Cd8a*, *Gbp4*, *P2ry14*, *Cd28*, *Cxcl9*), whereas both proinflammatory and anti-inflammatory secreted effectors were downregulated (*Ppbp*, *Cxcl3*, *Il6*, *F10*, *Cxcl1*, *Il1f9*, *Il10*, *Itga1*, *Clec4d*, *Olr1*, *Sphk1*, *Ednrb*). A strong decrease of expression of genes involved in transcription, translation, and lipid metabolism was observed (*Arg1*, *Agpat9*, *B3gnt5*, *Ero1l*, *Sgms2*, *Car5b*, *Avpi1*, *Gyk*, *Ell2*, *Car6*, *Agpat4*, *Gpd2*, *Odc1*, *Idi1*, *Padi4*, *Eif4e*, *Nop58*, *Mboat1*, *Eef1e1*). A complementary tool to analyze gene expression with time was to cluster the genes according to their kinetics of expression. Genes differentially expressed by Ly6C^pos macrophages gathered in only two main clusters that presented radical changes in gene expression profile between days 2 and 4 (Fig. 5). Accordingly, the GO enrichments observed in clusters 1 and 2 matched with those observed for downregulated and upregulated genes between days 2 and 4 depicted earlier. Although much less numerous from day 4, Ly6C^pos macrophages exhibited gene expression variations in some part similar to those of Ly6C^neg cells (see later) during the late steps of regeneration (Supplemental Table 4), indicating that the environment largely controls gene expression of this cell subset from day 4. Notably, because a single sample was available for Ly6C^pos cells at day 8, some variations between days 4 and 8, such as upregulation observed in some genes of cluster 1 (and exemplified in Fig. 4A), were not taken into account for this scarce population at this time point.

Dynamics of Ly6C^neg macrophages during the course of muscle regeneration

Horizontal analysis showed that Ly6C^neg cells upregulated genes, first associated with the preparation of proliferation and then with cell division, until day 4 (Supplemental Table 4), confirming the
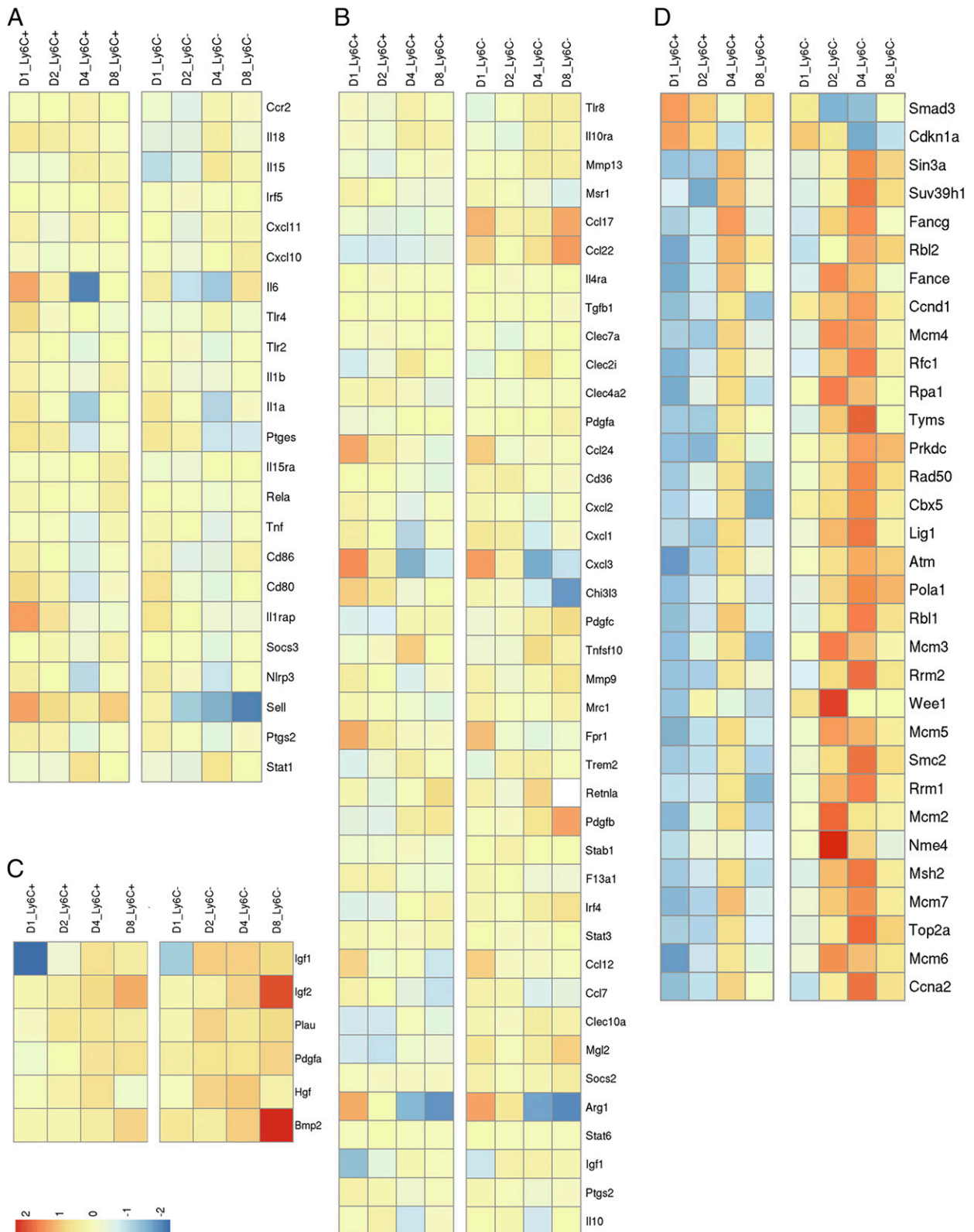
FIGURE 3. Analysis of inflammatory markers in Ly6C^pos versus Ly6C^neg macrophage subsets. Expression pattern of proinflammatory (**A**) and anti-inflammatory (**B**) markers of genes involved in myogenesis (**C**) and genes associated with cell cycle (**D**) by regenerating Ly6C^pos and Ly6C^neg muscle-derived macrophages.

earlier vertical analysis. GO terms related to response to wounding and immune response were variably regulated in Ly6C^neg macrophages but clearly showed a downregulation of genes associated with chemotaxis and cell motility in the early regenerating phases (see top/bottom genes in Supplemental Table 1) (e.g., *Fpr1*, *Cxcl3*,

Ccl24, *Itga1*, *Il6*, *Arg1*, *Clec4n*, *Ccl22*, *Pecam1*, *Itgal*, *Selp*). At later stages, GO categories including intracellular signal transduction associated with immune response and cell communication (regulation of cytokine production; Supplemental Table 4) were upregulated (e.g., *Itk*, *Ralgds*, *Adora2b*, *Arl5b*, *Map2k3*, *Fosl2*,
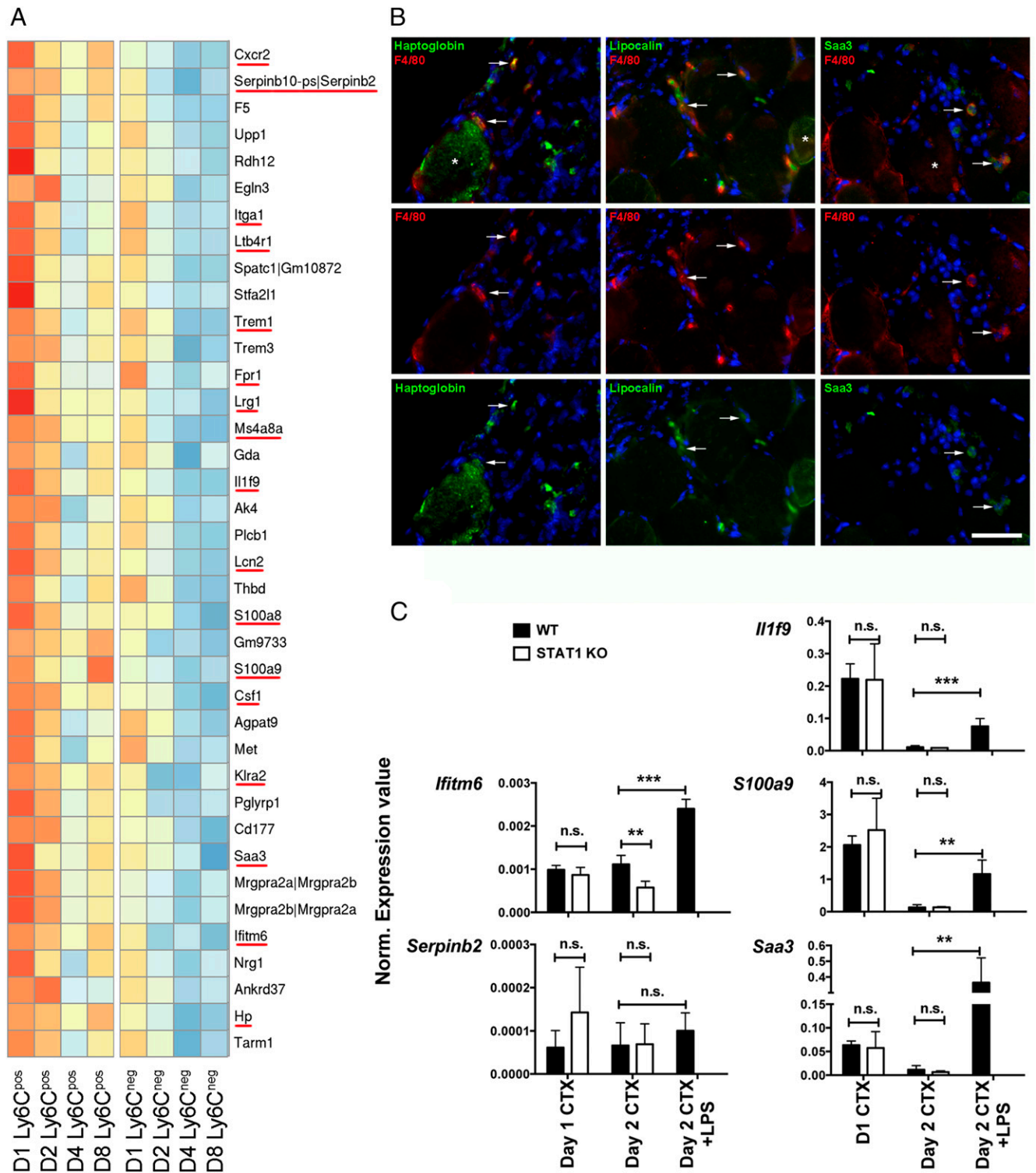
FIGURE 4. Genes highly expressed by infiltrating Ly6C^{pos} macrophages during early steps of muscle regeneration. (**A**) Heat map of genes upregulated by Ly6C^{pos} as compared with Ly6C^{neg} at day 1 after injury, including a series of genes associated with inflammation (underlined in red). (**B**) Immuno-histofluorescence showing the expression of acute-phase proteins (green) by F4/80^{pos} macrophages (red) in skeletal muscle day 2 after injury. Arrows show examples of double-labeled cells. Asterisks show necrotic myofibers trapping some Abs nonspecifically. Scale bar, 50 μm. (**C**) Real-time quantitative RT-PCR of genes highly expressed in Ly6C^{pos} macrophages at day 1 of regeneration in CD45^{pos} cells of WT and STAT1 knock-out mice at days 1 and 2 of muscle regeneration after CTX injection. In some experiments, LPS has been injected together with CTX in WT animals. Results are mean ± SEM of three independent experiments. **$p < 0.01$, ***$p < 0.001$.

Rab20, *Gem*, *Dusp16*, *Rapgef2*, and *Rcan1* for signal transduction and *Il6*, *vcam1*, *Il10*, *Cd81*, *Bmp2*, *Fasl*, *Ccl22*, *Pdgfb*, *Ctla4*, *Il1a*, *Malt1*, and *Tigit* for immune response) (Supplemental Table 1). Finally, genes associated with the metabolism of ribosomes/RNA,

glucose, and macromolecules were downregulated at the late steps of regeneration, indicating a metabolic shift in macrophage sub-sets during regeneration (Supplemental Table 4). Some of the most downregulated genes were related to the redox status (*Arg1*, *Odc1*,

Ly6C^pos macrophages

Ly6C^neg macrophages
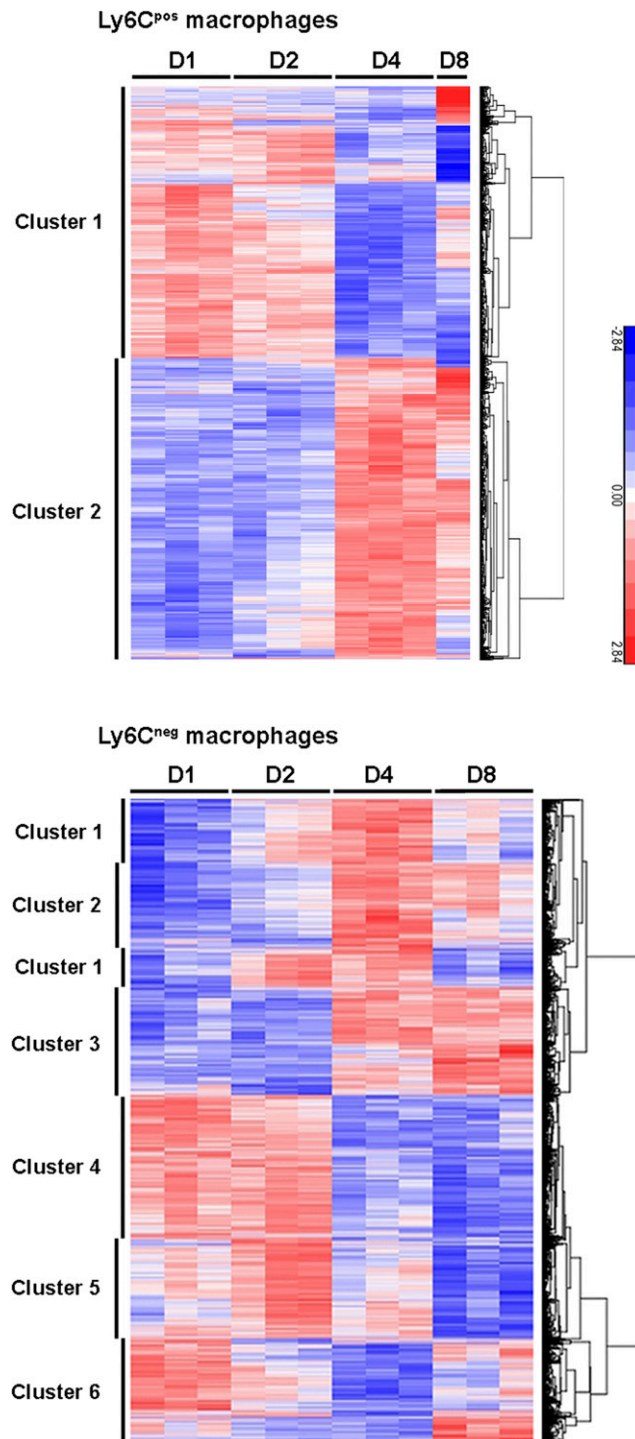
FIGURE 5. Clustering of genes according to their kinetics of expression. (**A**) Clustering of genes in Ly6C^pos macrophages revealed two main clusters. (**B**) Clustering of genes in Ly6C^neg macrophages revealed six clusters.

Car6, Mdm2, Srxn1, Ero1l, Txnrd1, Adssl1, Sod2, Rars, Gclc, Gpd2) (Supplemental Table 1).

Overall, the differentially regulated genes in Ly6C^neg cells clustered into six groups according to their kinetics of expression (Fig. 5). Clusters 4 and 5 contained genes highly expressed at days 1–2 of regeneration and were enriched for various GOs including RNA metabolism, transcription, translation, preparation of the cell to energy expenditure, and intracellular transport (Fig. 6, Supplemental Table 5). Genes showing a progressive (cluster 1) or strong (cluster

2) upregulation at day 4 showed enrichment in GOs associated with DNA packaging, macromolecule synthesis and assembly, and cell cycle (Fig. 6, Supplemental Table 5). Cluster 3 encompassed genes showing an upregulation with time, particularly between days 4 and 8, and was enriched for wound healing, regulation of cell activation, cytokine production, and cell communication GOs (Fig. 6, Supplemental Table 5). Cluster 6 gathered genes whose expression decreased until day 4 and strongly increased between days 4 and 8. Cluster 6 was enriched for GO terms associated with wound healing and cell communication including regulation of cell differentiation, response to signaling, and tissue remodeling, among which are secreted molecules (Fig. 6, Supplemental Table 5).

Metabolic shift of macrophages during skeletal muscle regeneration

The earlier horizontal analysis of macrophage profile suggested metabolic changes during muscle regeneration. Detailed metabolic regulation has been recently investigated in in vitro–activated macrophages and showed that M2(IL-4) macrophage profile was associated with glutamine metabolism, involved in activation of tricarboxylic acid (TCA) cycle and oxidative phosphorylation (15). Most of the genes (16/22) identified as being dependent on glutamine in Jha et al.'s study (15) were upregulated during the late steps of muscle regeneration (Fig. 7A), suggesting that oxidative metabolism is associated with Ly6C^neg macrophage functions that are more numerous at this time. Moreover, GSEA analysis against the KEGG database was performed for horizontal comparisons as in Jha et al.'s study. In both macrophage subsets (Supplemental Table 6), pathways that were upregulated between days 1 and 2 of regeneration were linked to oxidative metabolism (KEGG citrate cycle TCA cycle, KEGG oxidative phosphorylation, KEGG fatty acid metabolism, KEGG pyruvate metabolism, etc.). Most of these pathways were then downregulated from day 4 of muscle regeneration (Supplemental Table 6). These results indicate important metabolic changes in macrophages, with an upregulation of oxidative metabolism preceding the change of their inflammatory status.

Secretory profile of Ly6C^neg macrophages during the late steps of muscle regeneration

GO cell component enrichment of the 10% most differentially expressed genes revealed that clusters 3 and 6, encoding for genes upregulated at the end of the regeneration process, were enriched for extracellular/secreted products (Fig. 6). Among the most differentially regulated genes, several genes encoding for extracellular matrix (ECM) components and ECM remodeling proteins were observed. *Bgn* and *Postn*, encoding for two ECM proteins, were among the top-ranked upregulated genes in Ly6C^neg macrophages between days 2 and 4. Scrutinizing the entire list led to the identification of a set of ECM genes highly expressed by Ly6C^neg macrophages during the late phases of muscle regeneration (Fig. 7B). This indicates that macrophages are direct contributors of ECM reorganization during the healing phase of tissue repair.

Discussion

Macrophage plasticity is a major paradigm in innate immunology. In vitro experimental systems lack both the complex milieu present in vivo and the dynamic aspects of macrophage phenotype shifts. We have addressed this issue by taking advantage of a highly dynamic sterile inflammatory model, CTX-induced muscle regeneration, in which acute inflammation is rapidly followed by the resolution of inflammation and ensuing regeneration process. In this model, we have assessed the transcriptomes of macrophage populations,

FIGURE 6. GO analysis of clusters of genes expressed by Ly6C^{neg} macrophages. Clusters of genes showing the highest expression at days 2 (clusters 4 and 5), 4 (clusters 1 and 2), and 8 (clusters 6 and 3) of muscle regeneration were analyzed in DAVID for GO-biological processes and clustered with REViGO tool. Main GO clusters are represented in pie charts according to their significance. Details are presented in Supplemental Table 5. Histograms below the pie chart present, for each cluster, GO-Cell component enrichment. White bars represent GOs associated with genes coding for intracellular proteins; gray bars represent GOs associated with genes coding for membrane proteins; black bars represent GOs associated with genes coding for extracellular proteins.

which revealed unexpected highly dynamic changes of gene expression during acute inflammation and subsequent tissue repair, confirming the highly versatile nature of these cells.

We show that macrophages from regenerating muscle were distinct from resting macrophages in other tissues, while they exhibited a pronounced macrophage-like core expression signature, particu-
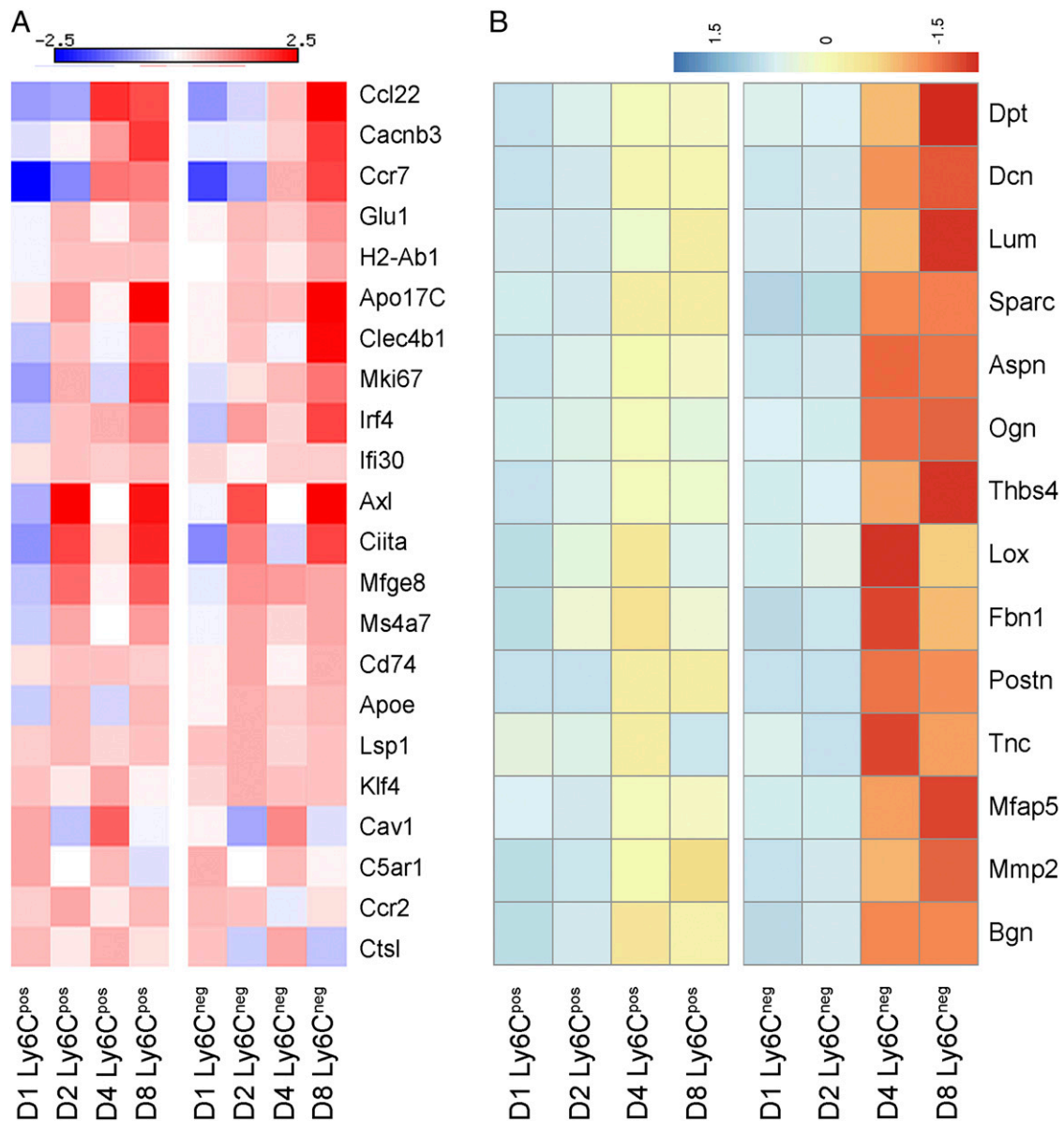
FIGURE 7. Metabolism- and ECM-related genes highly expressed in Ly6C^{neg} macrophages. (**A**) Heat maps of genes regulated by the presence of glutamine and associated with oxidative metabolism as described by Jha et al. (15) in Ly6C^{pos} and Ly6C^{neg} macrophages during muscle regeneration. (**B**) Heat maps of genes associated with ECM and ECM regulation, in Ly6C^{pos} and Ly6C^{neg} macrophages during muscle regeneration.

larly at late time points of regeneration. They also expressed at these late stages some DC markers, especially in the Ly6C^{neg} subset. Expression of DC markers by monocyte-derived macrophages has already been shown (5, 8), and some DC properties have been identified for macrophages in late regenerating muscle (31).

Analysis of gene expression revealed that the elapsed time, much more than Ly6C status, showed the highest differential gene expression in macrophages during muscle regeneration. Thus, the time course of inflammation is the predominant organizing force in gene expression by macrophages, with an important time point at days 2–4 postinjury, which corresponds to the full skewing from Ly6C^{pos} to Ly6C^{neg} status (13, 16) and the starting of resolution of inflammation. This result is a clear departure from the widely held assumption that the Ly6C$^{pos/neg}$ status is the predominant defining feature of these macrophages with strong predictive power for their molecular signature/functions. A highly related issue is the polarization status of the Ly6C$^{pos/neg}$ subsets, which have been assumed to correspond, as in other tissues, to M1 and M2 macro-

phages, respectively (13, 16, 23). We show that the damage-associated Ly6C^{pos} macrophages exhibited a specific inflammatory profile, independent of STAT1, which only partially overlapped with the broad M1 gene expression pattern and displayed a unique inflammatory signature during the early response to muscle injury (days 1–2), likely reporting sterile inflammation (see later). Similarly, Ly6C^{neg} macrophages were unsuccessfully linked to canonical M2(IL-4) macrophage. Although they preferentially expressed anti-inflammatory markers, their expression profile did not match with any of the in vitro activation status tested so far (3). Only partial overlap was observed with macrophages stimulated with fatty acids (3). These results indicate that in vivo macrophages cannot be restricted to the M1/M2 nomenclature during tissue injury/repair. Instead, we evidence four specific features that account for the high dynamic changes in gene expression observed in macrophages during muscle regeneration.

The first feature is early expression of acute-phase proteins by Ly6C^{pos} macrophages. Ly6C^{pos} macrophages entering the injured

muscle highly expressed genes involved in inflammation, including acute-phase proteins, such as SAA3, S100A8/9, Lipocalin-2, and Haptoglobin (32). Both pathogen-associated and damage-associated molecular pattern molecules induce macrophage expression of S100A8 and S100A9 (33), which dimerize to form calprotectin, which, in turn, triggers SAA3 expression (34) by macrophages (35–37). Interestingly, macrophage-derived calprotectin is an early contributor of skeletal muscle myositis, which is characterized by a huge inflammatory infiltrate (38) and is also upregulated after exercise (39), suggesting that these macrophage-derived proteins are crucial for launching the regeneration/remodeling process in skeletal muscle. Lipocalin-2 and haptoglobin are involved in the regulation of iron metabolism, by binding small iron-carrying molecules (siderophores) and hemoglobin (before internalization by CD163 receptor), respectively. Iron capture protects against iron-mediated toxicity (40). This is in agreement with the described iron retention phenotype of M1 macrophages (41), which also has been described in early regenerating muscle (42). It has been shown that chelatable iron release from disrupted muscle tissue represents the major cause for the oxidative stress that aggravates muscle destruction (43). Thus, high expression of iron-scavenging molecules by Ly6C^{pos} macrophages may favor iron elimination to protect the tissue.

Second, metabolic change of macrophages precedes and sustains the resolution of inflammation. Although metabolism is foreseen as an important regulator of macrophage function, notably in diseases (44), few studies addressed specific metabolic pathways linked to specific macrophage inflammatory status. The shift from M1 to M2 macrophages is associated with a change in glucose metabolism, with a reshuffling from glycolysis to oxidative metabolism (13, 45, 46). Accordingly, we observed at the time of resolution of inflammation (between days 2 and 4) a downregulation of genes associated with glycolysis and glucose metabolism in both Ly6C^{pos} and Ly6C^{neg} macrophages. This was preceded by an early upregulation, between days 1 and 2, of the pathways associated with oxidative phosphorylation and TCA cycle, suggesting that macrophages first started to shift their metabolic profile before shifting their inflammatory status. Finally, we observed a strong upregulation of genes involved in glutamine metabolism, associated with oxidative metabolism, which is characteristic of M2(IL-4) macrophages in vitro (15), during the late steps of muscle regeneration (days 4–8). These results suggest that metabolic shift precedes inflammatory shift in macrophages and that a specific metabolic signature characterizes recovery macrophages during the repair phase.

The third feature is proliferation of Ly6C^{neg} macrophages, which likely explains the high numbers of Ly6C^{neg} macrophages present in the muscle later on (12). Kinetic analysis showed the molecular foundation that allowed Ly6C^{neg} macrophages to get prepared for division at day 1 and to actively divide at days 2–4 of regeneration. Similarly, macrophage proliferation occurs at the time of resolution of inflammation in peritonitis (47). Moreover, expression of M-CSF, which is essential to macrophage proliferation (47), was highly enhanced in macrophages between days 2 and 4 of muscle regeneration (Supplemental Table 1).

The fourth feature is expression of ECM components by Ly6C^{neg} macrophages during the healing phase. Ly6C^{neg} macrophages expressed mainly secretory proteins at days 4–8 of regeneration, which are involved in intercellular communication. A specific enrichment was observed for ECM and ECM-regulating proteins, including proteoglycans, matricellular proteins, and assembly proteins. Interestingly, most of these molecules are involved in skeletal muscle regeneration and some of them are expressed by macrophages during tissue repair (Supplemental Table 7). These results suggest that macrophages directly participate in the synthesis and assembly/organization of ECM constituents.

In conclusion, this study highlights an unexpected dynamic nature of macrophage subset gene signature during skeletal muscle regeneration. Early-arriving Ly6C^{pos}CX3CR1^{lo} macrophages, which exhibit damage-associated, highly specialized molecular signature, sense and report tissue injury by producing acute-phase proteins, alarmins, and other factors. These macrophages early modify their cellular metabolism (downregulation of glycolysis pathway, upregulation of oxidative pathway), and later on their inflammatory phenotype, to become anti-inflammatory Ly6C^{neg}CX3CR1^{hi} macrophages. These latter actively divide while participating in a regeneration/healing process through the secretion of molecules involved in intercellular communications, notably ECM-related molecules, which are crucial for the recovery of muscle integrity. Ly6C^{neg}CX3CR1^{hi} macrophages fulfill the designation of restorative macrophages given their ability to produce proregenerative factors (e.g., insulin-like growth factor-1 [29]) and their contribution to muscle regeneration by acting on both myogenic (13) and fibroadipogenic (48) precursors.

Acknowledgments

Disclosures

The authors have no financial conflicts of interest.

References

1. Sica, A., and A. Mantovani. 2012. Macrophage plasticity and polarization: in vivo veritas. *J. Clin. Invest.* 122: 787–795.
2. Mantovani, A., S. K. Biswas, M. R. Galdiero, A. Sica, and M. Locati. 2013. Macrophage plasticity and polarization in tissue repair and remodelling. *J. Pathol.* 229: 176–185.
3. Xue, J., S. V. Schmidt, J. Sander, A. Draffehn, W. Krebs, I. Quester, D. De Nardo, T. D. Gohel, M. Emde, L. Schmidleithner, et al. 2014. Transcriptome-based network analysis reveals a spectrum model of human macrophage activation. *Immunity* 40: 274–288.
4. Hilgendorf, I., L. M. Gerhardt, T. C. Tan, C. Winter, T. A. Holderried, B. G. Chousterman, Y. Iwamoto, R. Liao, A. Zirlik, M. Scherer-Crosbie, et al. 2014. Ly-6Chigh monocytes depend on Nr4a1 to balance both inflammatory and reparative phases in the infarcted myocardium. *Circ. Res.* 114: 1611–1622.
5. Zigmond, E., C. Varol, J. Farache, E. Elmaliah, A. T. Satpathy, G. Friedlander, M. Mack, N. Shpigel, I. G. Boneca, K. M. Murphy, et al. 2012. Ly6C hi monocytes in the inflamed colon give rise to proinflammatory effector cells and migratory antigen-presenting cells. *Immunity* 37: 1076–1090.
6. Geissmann, F., S. Jung, and D. R. Littman. 2003. Blood monocytes consist of two principal subsets with distinct migratory properties. *Immunity* 19: 71–82.
7. Dal-Secco, D., J. Wang, Z. Zeng, E. Kolaczkowska, C. H. Wong, B. Petri, R. M. Ransohoff, I. F. Charo, C. N. Jenne, and P. Kubes. 2015. A dynamic spectrum of monocytes arising from the in situ reprogramming of CCR2+ monocytes at a site of sterile injury. *J. Exp. Med.* 212: 447–456.
8. Stables, M. J., S. Shah, E. B. Camon, R. C. Lovering, J. Newson, J. Bystrom, S. Farrow, and D. W. Gilroy. 2011. Transcriptomic analyses of murine resolution-phase macrophages. *Blood* 118: e192–e208.
9. Gautier, E. L., T. Shay, J. Miller, M. Greter, C. Jakubzick, S. Ivanov, J. Helft, A. Chow, K. G. Elpek, S. Gordonov, et al; Immunological Genome Consortium. 2012. Gene-expression profiles and transcriptional regulatory pathways that underlie the identity and diversity of mouse tissue macrophages. *Nat. Immunol.* 13: 1118–1128.
10. Lavin, Y., D. Winter, R. Blecher-Gonen, E. David, H. Keren-Shaul, M. Merad, S. Jung, and I. Amit. 2014. Tissue-resident macrophage enhancer landscapes are shaped by the local microenvironment. *Cell* 159: 1312–1326.
11. Gosselin, D., V. M. Link, C. E. Romanoski, G. J. Fonseca, D. Z. Eichenfield, N. J. Spann, J. D. Stender, H. B. Chun, H. Garner, F. Geissmann, and C. K. Glass. 2014. Environment drives selection and function of enhancers controlling tissue-specific macrophage identities. [Published erratum appears in 2015 *Cell* 160: 351–352.] *Cell* 159: 1327–1340.
12. Arnold, L., A. Henry, F. Poron, Y. Baba-Amer, N. van Rooijen, A. Plonquet, R. K. Gherardi, and B. Chazaud. 2007. Inflammatory monocytes recruited after skeletal muscle injury switch into antiinflammatory macrophages to support myogenesis. *J. Exp. Med.* 204: 1057–1069.

13. Mounier, R., M. Théret, L. Arnold, S. Cuvellier, L. Bultot, O. Göransson, N. Sanz, A. Ferry, K. Sakamoto, M. Foretz, et al. 2013. AMPKα1 regulates macrophage skewing at the time of resolution of inflammation during skeletal muscle regeneration. *Cell Metab.* 18: 251–264.

14. Subramanian, A., P. Tamayo, V. K. Mootha, S. Mukherjee, B. L. Ebert, M. A. Gillette, A. Paulovich, S. L. Pomeroy, T. R. Golub, E. S. Lander, and J. P. Mesirov. 2005. Gene set enrichment analysis: a knowledge-based approach for interpreting genome-wide expression profiles. *Proc. Natl. Acad. Sci. USA* 102: 15545–15550.

15. Jha, A. K., S. C. Huang, A. Sergushichev, V. Lampropoulou, Y. Ivanova, E. Loginicheva, K. Chmielewski, K. M. Stewart, J. Ashall, B. Everts, et al. 2015. Network integration of parallel metabolic and transcriptional data reveals metabolic modules that regulate macrophage polarization. *Immunity* 42: 419–430.

16. Perdiguero, E., P. Sousa-Victor, V. Ruiz-Bonilla, M. Jardí, C. Caelles, A. L. Serrano, and P. Muñoz-Cánoves. 2011. p38/MKP-1-regulated AKT coordinates macrophage transitions and resolution of inflammation during tissue repair. *J. Cell Biol.* 195: 307–322.

17. Murphy, M. M., J. A. Lawson, S. J. Mathew, D. A. Hutcheson, and G. Kardon. 2011. Satellite cells, connective tissue fibroblasts and their interactions are crucial for muscle regeneration. *Development* 138: 3625–3637.

18. Le Grand, F., R. Grifone, P. Mourikis, C. Houbron, C. Gigaud, J. Pujol, M. Maillet, G. Pagès, M. Rudnicki, S. Tajbakhsh, and P. Maire. 2012. Six1 regulates stem cell repair potential and self-renewal during skeletal muscle regeneration. *J. Cell Biol.* 198: 815–832.

19. Saclier, M., S. Cuvellier, M. Magnan, R. Mounier, and B. Chazaud. 2013. Monocyte/macrophage interactions with myogenic precursor cells during skeletal muscle regeneration. *FEBS J.* 280: 4118–4130.

20. Miller, J. C., B. D. Brown, T. Shay, E. L. Gautier, V. Jojic, A. Cohain, G. Pandey, M. Leboeuf, K. G. Elpek, J. Helft, et al; Immunological Genome Consortium. 2012. Deciphering the transcriptional network of the dendritic cell lineage. *Nat. Immunol.* 13: 888–899.

21. Ritchie, M. E., B. Phipson, D. Wu, Y. Hu, C. W. Law, W. Shi, and G. K. Smyth. 2015. limma powers differential expression analyses for RNA-sequencing and microarray studies. *Nucleic Acids Res.* 43: e47.

22. Varga, T., R. Mounier, P. Gogolak, S. Poliska, B. Chazaud, and L. Nagy. 2013. Tissue LyC6- macrophages are generated in the absence of circulating LyC6- monocytes and Nur77 in a model of muscle regeneration. *J. Immunol.* 191: 5695–5701.

23. Wang, H., D. W. Melton, L. Porter, Z. U. Sarwar, L. M. McManus, and P. K. Shireman. 2014. Altered macrophage phenotype transition impairs skeletal muscle regeneration. *Am. J. Pathol.* 184: 1167–1184.

24. Christov, C., F. Chrétien, R. Abou-Khalil, G. Bassez, G. Vallet, F. J. Authier, Y. Bassaglia, V. Shinin, S. Tajbakhsh, B. Chazaud, and R. K. Gherardi. 2007. Muscle satellite cells and endothelial cells: close neighbors and privileged partners. *Mol. Biol. Cell* 18: 1397–1409.

25. Lu, H., D. Huang, N. Saederup, I. F. Charo, R. M. Ransohoff, and L. Zhou. 2011. Macrophages recruited via CCR2 produce insulin-like growth factor-1 to repair acute skeletal muscle injury. *FASEB J.* 25: 358–369.

26. Novak, M. L., S. C. Bryer, M. Cheng, M. H. Nguyen, K. L. Conley, A. K. Cunningham, B. Xue, T. H. Sisson, J. S. You, T. A. Hornberger, and T. J. Koh. 2011. Macrophage-specific expression of urokinase-type plasminogen activator promotes skeletal muscle regeneration. *J. Immunol.* 187: 1448–1457.

27. Schulze, M., F. Belema-Bedada, A. Technau, and T. Braun. 2005. Mesenchymal stem cells are recruited to striated muscle by NFAT/IL-4-mediated cell fusion. *Genes Dev.* 19: 1787–1798.

28. Sisson, T. H., M. H. Nguyen, B. Yu, M. L. Novak, R. H. Simon, and T. J. Koh. 2009. Urokinase-type plasminogen activator increases hepatocyte growth factor activity required for skeletal muscle regeneration. *Blood* 114: 5052–5061.

29. Tonkin, J., L. Temmerman, R. D. Sampson, E. Gallego-Colon, L. Barberi, D. Bilbao, M. D. Schneider, A. Musarò, and N. Rosenthal. 2015. Monocyte/macrophage-derived IGF-1 orchestrates murine skeletal muscle regeneration and modulates autocrine polarization. *Mol. Ther.* 23: 1189–1200.

30. Murray, P. J., J. E. Allen, S. K. Biswas, E. A. Fisher, D. W. Gilroy, S. Goerdt, S. Gordon, J. A. Hamilton, L. B. Ivashkiv, T. Lawrence, et al. 2014. Macrophage activation and polarization: nomenclature and experimental guidelines. [Published erratum appears in 2014 *Immunity* 41: 339–340.] *Immunity* 41: 14–20.

31. Brigitte, M., C. Schilte, A. Plonquet, Y. Baba-Amer, A. Henri, C. Charlier, S. Tajbakhsh, M. Albert, R. K. Gherardi, and F. Chrétien. 2010. Muscle resident macrophages control the immune cell reaction in a mouse model of notexin-induced myoinjury. *Arthritis Rheum.* 62: 268–279.

32. Gabay, C., and I. Kushner. 1999. Acute-phase proteins and other systemic responses to inflammation. *N. Engl. J. Med.* 340: 448–454.

33. Goyette, J., and C. L. Geczy. 2011. Inflammation-associated S100 proteins: new mechanisms that regulate function. *Amino Acids* 41: 821–842.

34. Hiratsuka, S., A. Watanabe, Y. Sakurai, S. Akashi-Takamura, S. Ishibashi, K. Miyake, M. Shibuya, S. Akira, H. Aburatani, and Y. Maru. 2008. The S100A8-serum amyloid A3-TLR4 paracrine cascade establishes a pre-metastatic phase. *Nat. Cell Biol.* 10: 1349–1355.

35. Meek, R. L., N. Eriksen, and E. P. Benditt. 1992. Murine serum amyloid A3 is a high density apolipoprotein and is secreted by macrophages. *Proc. Natl. Acad. Sci. USA* 89: 7949–7952.

36. Anthony, D., J. L. McQualter, M. Bishara, E. X. Lim, S. Yatmaz, H. J. Seow, M. Hansen, M. Thompson, J. A. Hamilton, L. B. Irving, et al. 2014. SAA drives proinflammatory heterotypic macrophage differentiation in the lung via CSF-1R-dependent signaling. *FASEB J.* 28: 3867–3877.

37. Jang, E., S. Lee, J. H. Kim, J. H. Kim, J. W. Seo, W. H. Lee, K. Mori, K. Nakao, and K. Suk. 2013. Secreted protein lipocalin-2 promotes microglial M1 polarization. *FASEB J.* 27: 1176–1190.

38. Rostasy, K. M., M. Piepkorn, H. H. Goebel, S. Menck, F. Hanefeld, and W. J. Schulz-Schaeffer. 2004. Monocyte/macrophage differentiation in dermatomyositis and polymyositis. *Muscle Nerve* 30: 225–230.

39. Mortensen, O. H., K. Andersen, C. Fischer, A. R. Nielsen, S. Nielsen, T. Akerström, M. B. Aastrøm, R. Borup, and B. K. Pedersen. 2008. Calprotectin is released from human skeletal muscle tissue during exercise. *J. Physiol.* 586: 3551–3562.

40. Thomsen, J. H., A. Etzerodt, P. Svendsen, and S. K. Moestrup. 2013. The haptoglobin-CD163-heme oxygenase-1 pathway for hemoglobin scavenging. *Oxid. Med. Cell. Longev.* 2013: 523652.

41. Cairo, G., S. Recalcati, A. Mantovani, and M. Locati. 2011. Iron trafficking and metabolism in macrophages: contribution to the polarized phenotype. *Trends Immunol.* 32: 241–247.

42. Corna, G., L. Campana, E. Pignatti, A. Castiglioni, E. Tagliafico, L. Bosurgi, A. Campanella, S. Brunelli, A. A. Manfredi, P. Apostoli, et al. 2010. Polarization dictates iron handling by inflammatory and alternatively activated macrophages. *Haematologica* 95: 1814–1822.

43. Kerkweg, U., K. Pamp, J. Fieker, F. Petrat, R. C. Hider, and H. de Groot. 2010. Release of redox-active iron by muscle crush trauma: no liberation into the circulation. *Shock* 33: 513–518.

44. Biswas, S. K., and A. Mantovani. 2012. Orchestration of metabolism by macrophages. *Cell Metab.* 15: 432–437.

45. Haschemi, A., P. Kosma, L. Gille, C. R. Evans, C. F. Burant, P. Starkl, B. Knapp, R. Haas, J. A. Schmid, C. Jandl, et al. 2012. The sedoheptulose kinase CARKL directs macrophage polarization through control of glucose metabolism. *Cell Metab.* 15: 813–826.

46. Tan, Z., N. Xie, H. Cui, D. R. Moellering, E. Abraham, V. J. Thannickal, and G. Liu. 2015. Pyruvate dehydrogenase kinase 1 participates in macrophage polarization via regulating glucose metabolism. *J. Immunol.* 194: 6082–6089.

47. Davies, L. C., M. Rosas, S. J. Jenkins, C. T. Liao, M. J. Scurr, F. Brombacher, D. J. Fraser, J. E. Allen, S. A. Jones, and P. R. Taylor. 2013. Distinct bone marrow-derived and tissue-resident macrophage lineages proliferate at key stages during inflammation. *Nat. Commun.* 4: 1886.

48. Lemos, D. R., F. Babaeijandaghi, M. Low, C. K. Chang, S. T. Lee, D. Fiore, R. H. Zhang, A. Natarajan, S. A. Nedospasov, and F. M. Rossi. 2015. Nilotinib reduces muscle fibrosis in chronic muscle injury by promoting TNF-mediated apoptosis of fibro/adipogenic progenitors. *Nat. Med.* 21: 786–794.